PERGAMON

International Journal of Solids and Structures 38 (2001) 3377–3391

INTERNATIONAL JOURNAL OF SOLIDS and STRUCTURES

www.elsevier.com/locate/ijsolstr

Analysis of out-of-plane displacement and stress field in a piezocomposite plate with functionally graded microstructure

Abdulhakim Almajid, Minoru Taya *, Steven Hudnut

Department of mechanical engineering, Center for Intelligent Materials and Systems, University of Washington, Seattle, Washington 98195, USA

Received 4 October 1999; in revised form 24 March 2000

Abstract

A modified classical lamination theory (CLT) to account for piezoelectric coupling terms under applied electric field was developed. CLT is capable of predicting the stress field and out-of-plane displacement of laminated piezoelectric layers. CLT was applied to predict the stress and out-of-plane displacement of different types of piezoelectric actuators. A standard piezoelectric bimorph and a newly proposed piezoelectric functionally graded microstructure (FGM) bimorph were analyzed using CLT. The FGM piezoelectric laminates are composite materials whose electroelastic properties are varied through their thickness. The electroelastic properties of an FGM are made to vary in a linear or non-linear manner through the thickness to achieve the maximum displacement of the actuator while minimizing the induced stress field. The CLT results were verified using the finite element method.

Keywords: Piezoelectric composites; Functionally graded material; Piezoelectric actuator; Multi-layer piezoelectric actuator

1. Introduction

Piezoelectric composites have been used in a wide variety of applications including vibration control and actuators. Vibration control can be achieved by incorporating a thin piezoelectric layer into a structural system as analyzed by Tzou and Garde (1989) for the case of a thin laminate coupled with piezoelectric shell actuator. Crawley and Anderson (1990) distinguish the uniform strain bending from Bernoulli–Euler bending. Zhou and Tiersten (1994) used a variational method of elementary flexure and extension of composite plates to analyze a thin piezoelectric film incorporated in a structural system. Tauchert (1992) demonstrated the piezoelectric effect to suppress the thermally induced flexure of the laminate using classical lamination theory (CLT), however, the electroelastic properties were not reduced from 3-D to 2-D to account for the plane stress condition.

Several different kinds of piezoelectric actuators have been designed. Uchino et al. (1987) fabricated a monomorph made from semiconductive piezoelectric ceramics. A rainbow type actuator was developed by

* Corresponding author. Tel.: +1-206-685-2850; fax: +1-206-685-8047.
E-mail address: tayam@u.washington.edu (M. Taya).

0020-7683/01/$ - see front matter
PII: S0020-7683(00)00264-X

reducing one surface of a PZT wafer (Haertling, 1994). Wu et al. (1996) fabricated a piezoelectric actuator where the electrical resistivity was graded through the plate thickness leading to a graded poling of the material. However, stress concentration at the interface between the layers reduce the lifetime of these devices.

Functionally graded microstructure (FGM) in a ceramic/metal composite has been found to reduce the otherwise high thermal stress field at the interface between ceramic and metal plates (Taya et al., 1997). The concept of FGM can be applied to a piezolaminate plate by stacking piezoelectric composites of different compositions on top of each other. Chatterjee et al. (1999) have developed a multi-layered rainbow type actuator with graded piezoelectric properties through the thickness.

Each lamina within an FGM piezolaminate can be composed of either a uniform piezoelectric material or a composite of piezoelectric fillers and a piezoelectric or non-piezoelectric matrix. If the laminae in the FGM piezolaminate are composed of composites, then the electroelastic properties of each lamina must be accurately predicted. Micromechanical models to predict the electroelastic properties have been established (Dunn and Taya, 1993a,b).

In this paper, a modified CLT to account for piezoelectric coupling terms under applied electric field is developed. Mechanical and piezoelectric properties are reduced to a 2-D case from the original 3-D stiffness and piezoelectric matrices. CLT is then applied to predict the out-of-plane displacement and stress field of different types of actuators such as the standard bimorph and the FGM bimorph. Stress fields and out-of plane displacement for a laminated plate and a laminated cantilever beam were both investigated. The laminated plate is analyzed using CLT while the cantilever beam is analyzed using a reduced CLT for a 1-D model. The out-of-plane displacement and stress field were then verified against an finite element method (FEM) model.

2. Lamination model

A piezoelectric laminate consists of n laminae, each being a piezoelectric material with specified electroelastic properties. The constitutive equations of a piezoelectric material in the absence of temperature effects are given by

$$\sigma_{ij} = C_{ijkl}\varepsilon_{kl} - e_{mij}E_m, \tag{1}$$

where σ_{ij}, ε_{kl} are the stress and strain tensor components, respectively, E_m, the electric field vector component, C_{ijkl}, the elastic stiffness tensor, and e_{mij}, the piezoelectric coefficients. The electroelastic constants of each lamina may be computed from some micromechanical model such as the Eshelby type method as outlined by Dunn and Taya (1993a,b).

2.1. Laminated plate

CLT, as found in any composite textbook such as Gibson 1994, assumes a state of plane stress along the z-axis, where $\sigma_z = \sigma_{xz} = \sigma_{yz} = 0$. The constitutive equations of a piezoelectric lamina, Eq. (1), under applied electric field in the z-direction only (E_z), and under the assumption of plane stress along the z-axis, reduce to

$$\begin{Bmatrix} \sigma_x \\ \sigma_y \\ \sigma_{xy} \end{Bmatrix} = \begin{bmatrix} \overline{Q}_{11} & \overline{Q}_{12} & 0 \\ \overline{Q}_{21} & \overline{Q}_{22} & 0 \\ 0 & 0 & Q_{66} \end{bmatrix}_i \begin{Bmatrix} \varepsilon_x^0 + z\kappa_x \\ \varepsilon_y^0 + z\kappa_y \\ \gamma_{xy}^0 + z\kappa_{xy} \end{Bmatrix} - \begin{bmatrix} 0 & 0 & \overline{e}_{31} \\ 0 & 0 & \overline{e}_{32} \\ 0 & 0 & 0 \end{bmatrix} \begin{Bmatrix} 0 \\ 0 \\ E_z \end{Bmatrix}, \tag{2}$$

where

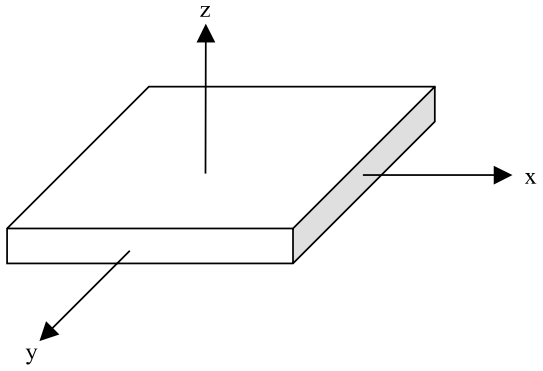

Fig. 1. Schematic view of piezoelectric plate.

$$\begin{aligned}\overline{Q}_{ij} &= C_{ij} - \frac{C_{i3}}{C_{33}} C_{j3}, \\ \overline{e}_{ij} &= \frac{C_{i3}}{C_{33}} e_{33} - e_{ij}.\end{aligned} \tag{3}$$

It is noted here that $\overline{Q}_{ij}$, $\overline{e}_{ij}$ are the reduced stiffness constants and reduced piezoelectric constants, respectively, that are modified by the assumption of plane stress and where ε_x^0, ε_y^0, and ε_{xy}^0 are the in-plane strain components at mid-plane, $z = 0$ as shown in Fig. 1, κ_x, κ_y, and κ_{xy} are the curvatures of the plate. These reduced properties can be obtained as explained in Appendix A. It is noted that Tauchert (1992) did not use the reduced stiffness and piezoelectric matrices, but he instead used the properties from the 3-D stiffness and piezoelectric matrices in a 2-D analysis, and that will lead to an incorrect solution.

The resultant in-plane forces and bending moments are defined by

$$\{N, M\} = \sum_{i=1}^{n} \int_{h_{i-1}}^{h_i} \{\sigma\}(\mathrm{d}z, z\,\mathrm{d}z). \tag{4}$$

Carrying out the integration through the plate thickness of h, the resultant forces and bending moments can then be written as

$$\begin{bmatrix} N \\ M \end{bmatrix} = \begin{bmatrix} A & B \\ B & D \end{bmatrix} \begin{Bmatrix} \varepsilon^0 \\ \kappa \end{Bmatrix} - \begin{bmatrix} N^E \\ M^E \end{bmatrix}, \tag{5}$$

where

$$[A, B, D] = \sum_{i=1}^{n} \int_{h_{i-1}}^{h_i} \left[\overline{Q}\right]_i \left(\mathrm{d}z, z\,\mathrm{d}z, z^2\,\mathrm{d}z\right), \tag{6a}$$

$$[N, M]^E = \sum_{i=1}^{n} \int_{h_{i-1}}^{h_i} [\overline{e}]_i \{E\}(\mathrm{d}z, z\,\mathrm{d}z), \tag{6b}$$

where h_{i-1} and h_i are the distance from the bottom of the plate to the bottom and top interfaces of the ith lamina, respectively, with $i = 1, 2, \ldots, n$. Hence the thickness of the ith lamina is then $h_i - h_{i-1}$. Under the applied electric field or temperature change only, i.e. $M = N = 0$ in Eq. (5), the in-plane strain and curvature can be solved as

$$\begin{bmatrix} \varepsilon^0 \\ \kappa \end{bmatrix} = \begin{bmatrix} a & b \\ b & d \end{bmatrix} \begin{bmatrix} N^E \\ M^E \end{bmatrix}, \tag{7}$$

where

$$\begin{bmatrix} a & b \\ b & d \end{bmatrix} = \begin{bmatrix} A & B \\ B & D \end{bmatrix}^{-1}.$$

Under a given electric field throughout the laminate, one can then predict the stress and displacement field of each layer as well as the out-of-plane displacement of the composite plate.

2.2. Laminated cantilever beam

In a laminated cantilever beam, an additional state of plane stress is assumed along the y-axis such that $\sigma_y = \sigma_{xy} = 0$. The constitutive equations in a piezoelectric lamina under applied electric field and uniform temperature then reduce to

$$\sigma_x = E_i\left(\varepsilon_x^0 + z\kappa_x\right) - e_i E_z, \tag{8}$$

where

$$\begin{aligned} E &= \left(C_{11} - \frac{C_{13}}{C_{33}}C_{13}\right) - \frac{\left(C_{12} - \frac{C_{13}}{C_{33}}C_{13}\right)^2}{\left(C_{11} - \frac{C_{13}}{C_{33}}C_{13}\right)}, \\ e &= \frac{\left(C_{12} - \frac{C_{13}}{C_{33}}C_{13}\right)}{\left(C_{11} - \frac{C_{13}}{C_{33}}C_{13}\right)}\left(\frac{C_{13}}{C_{33}}e_{33} - e_{13}\right) - \left(\frac{C_{13}}{C_{33}}e_{33} - e_{13}\right) \end{aligned} \tag{9}$$

and ε_x^0 are the mid-plane strain components at $z = 0$, while κ_x is the curvature of the beam. It is noted here that E and e are the reduced stiffness and piezoelectric constants, respectively, that have been modified by the assumption of 1-D beam theory model, as described in Appendix B. Following the same procedure outlined in the previous section and by substituting E and e instead of the $\overline{Q}$ and $\overline{e}$ matrices, the mid-plane strain and curvature can then be obtained.

3. Results

As an example of piezoelectric laminates, we shall consider piezoelectric laminates with a FGM, shown in Fig. 2, where the electroelastic properties of the laminae are varied smoothly from layer to layer. Four cases of piezoelectric laminate have been investigated. The first case is a standard bimorph where the top and bottom layers are both piezoelectric with either opposite polarity or opposite applied electric field as shown in Fig. 3(a). The second case represents a one-sided FGM laminate consisting of five distinct piezoelectric layers and in this case, the electric field is applied through the thickness of the entire laminate as shown in Fig. 3(b). The last two cases are a combination of a standard bimorph and an FGM by combining two FGM laminates to create a symmetric FGM bimorph (Fig. 3(c)). The reason for this is to increase the out-of-plane displacement by using a bimorph and also to decrease the stress concentration by using the concept of FGM. The two types of FGM bimorph studied were the type A as shown in Fig. 4(a), where the electroelastic properties increase toward the middle of the plate, and the type B (Fig. 4(b)), where the electroelastic properties decrease toward the middle of the plate. The distribution of the mechanical and piezoelectric properties were assumed to vary throughout the FGM plate as shown in Fig. 5, where the case

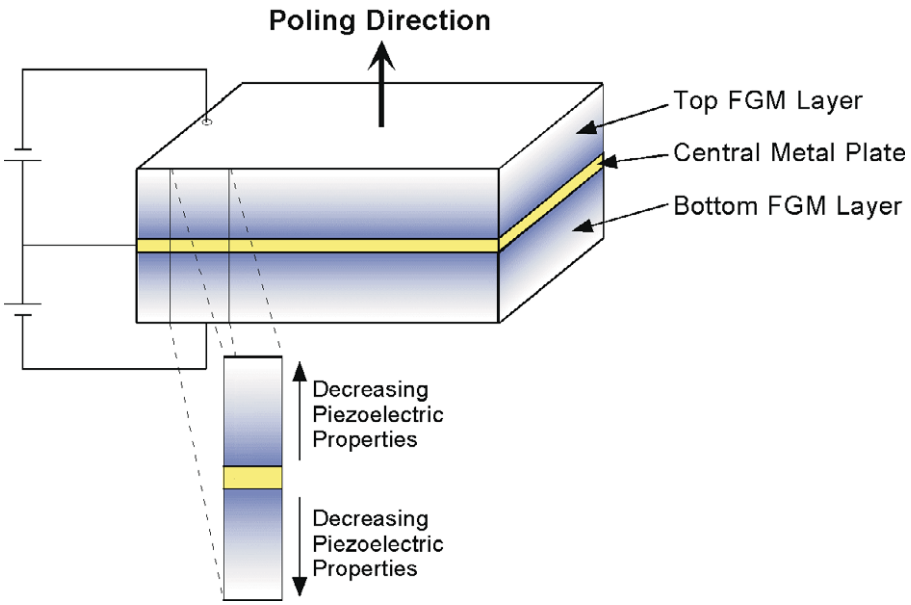

Fig. 2. Schematic of FGM bimorph type actuator.

Fig. 3. Different types of FGM.

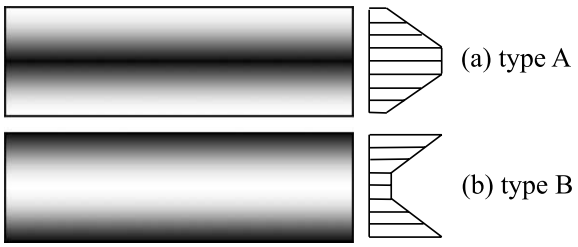

Fig. 4. Electroelastic properties distribution in FGM-bimorph.

of linear distribution in a one-sided FGM plate is illustrated schematically. The distribution starts with the lowest stiffness and least piezoelectric layer and increases linearly toward the highest stiffness and most piezoelectric layer. There are five layers within the FGM and therefore five distinct layers are presented with each layer having constant properties throughout its thickness. The elastic and piezoelectric properties of the piezoelectric composites were arbitrarily chosen as a linear function of the pure piezoelectric material and expressed as

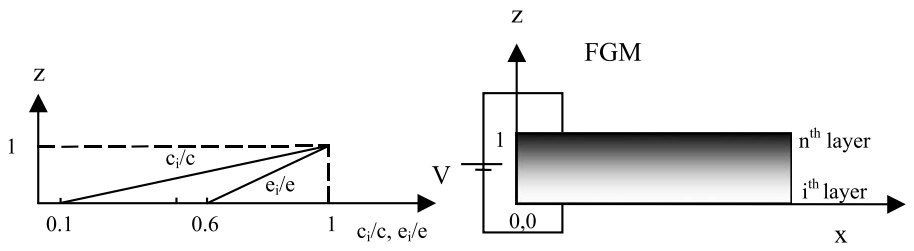

Fig. 5. The distribution of mechanical and piezoelectric properties in the FGM.

Table 1
Elastic and piezoelectric properties

	C_{11} (GPa)	C_{12} (GPa)	C_{13} (GPa)	C_{33} (GPa)	C_{44} (GPa)	e_{31} (C/m^2)	e_{33} (C/m^2)	E_{15} (C/m^2)
PZT-5A	121	75.4	75.2	111	21.1	−5.4	15.8	12.3
Au	101.43	41.63	41.63	101.43	29.9	0	0	0

$$\begin{aligned} C_i &= [0.1 + 0.225(i-1)]C_{\mathrm{PZT}}, \\ e_i &= [0.6 + 0.1(i-1)]e_{\mathrm{PZT}}, \end{aligned} \quad i = 1, 2, \ldots, n, \tag{10}$$

where C_i and e_i are the elastic and piezoelectric properties of the ith layer, respectively. C_{PZT} and e_{PZT} are the mechanical and piezoelectric properties of the pure piezoelectric material. The distribution of the FGM properties is chosen for comparison reasons within this paper only, and it may not represent the real distribution within an actual FGM as this will be subjected to fabrication capabilities. The electroelastic properties of the piezoelectric material and the gold layer at the mid-plane are given in Table 1.

3.1. Laminated plate

The analysis of the laminated plate is based on CLT under a state of plane stress along the z-axis. The stresses and displacement fields for each case that has been studied are presented in Table 2. The results are for a laminated plate clamped at one end and free at the other end (cantilever). The out-of-plane displacement was predicted for a plate length of 50 mm and a thickness of 0.5 mm for all cases. The thickness of each lamina within the FGM bimorph is 41 μm. The thickness of the mid-plane gold layer, which also

Table 2
Comparison of analytical results for out-of-plane displacement and in-plane stress of various types of piezocomposite clamped plates

Type of FGM microstructure	Standard bimorph, Fig. 2(a)	FGM one-sided, Fig. 2(b)	Bimorph FGM, Fig. 4(a) type A	Bimorph FGM, Fig. 4(b) type B
Electric field (V/mm)	1000	1000	1000	1000
Applied voltage (V)	208	500	208	208
Laminate thickness (mm)	0.5	0.5	0.5	0.5
No. of layers	2	5	10	10
Layer thickness (mm)	0.208, Au = 0.082	0.1	0.0416, Au = 0.082	0.0416, Au = 0.082
Curvature (1/m)	0.99	0.99	2.15	0.773
Maximum σ_x (MPa)	12.18	8.5	9.8	9.36
Deflection (mm) for plate length of 50 mm	1.24	1.245	2.7	0.97

serves as the central electrode, is 82 μm in all of the bimorphs. The electric field applied in all cases is 1000 V/mm.

The one-sided FGM plate was found to have the minimum in-plane stress of 8.5 MPa while the standard bimorph has maximum in-plane stresses of 12.1 MPa. The highest out-of-plane displacement was found to be 2.7 mm in the FGM bimorph, type A, where the properties increase toward the middle of the plate. This was about 120% higher than the 1.24 mm found in the standard bimorph, while at the same time, the in-plane stresses of 9.8 MPa in the FGM bimorph, type A, are 30% less than was found in the standard bimorph. The stress field profile of each case is presented in Fig. 6. In both the standard and FGM bimorphs, the magnitude of the in-plane stress increased toward the mid-plane as was expected. The interlaminar shear stresses associated with the in-plane stresses will be found by using a more accurate model such as FEM, since the lamination model cannot treat the interlaminar shear stress.

The FGM bimorph, type A, was the best choice among the cases that have been investigated. The use of linear versus non-linear distribution of the FGM properties is now considered. Three different distributions of the FGM properties as illustrated schematically in Fig. 7 are studied.

(1) Linear as in the previous case, Fig. 7(a)

$$\begin{aligned} C_i &= [0.1 + 0.225(i-1)]C_{\mathrm{PZT}}, \\ e_i &= [0.6 + 0.1(i-1)]e_{\mathrm{PZT}}, \end{aligned} \qquad i = 1, 2, \ldots, n, \tag{11}$$

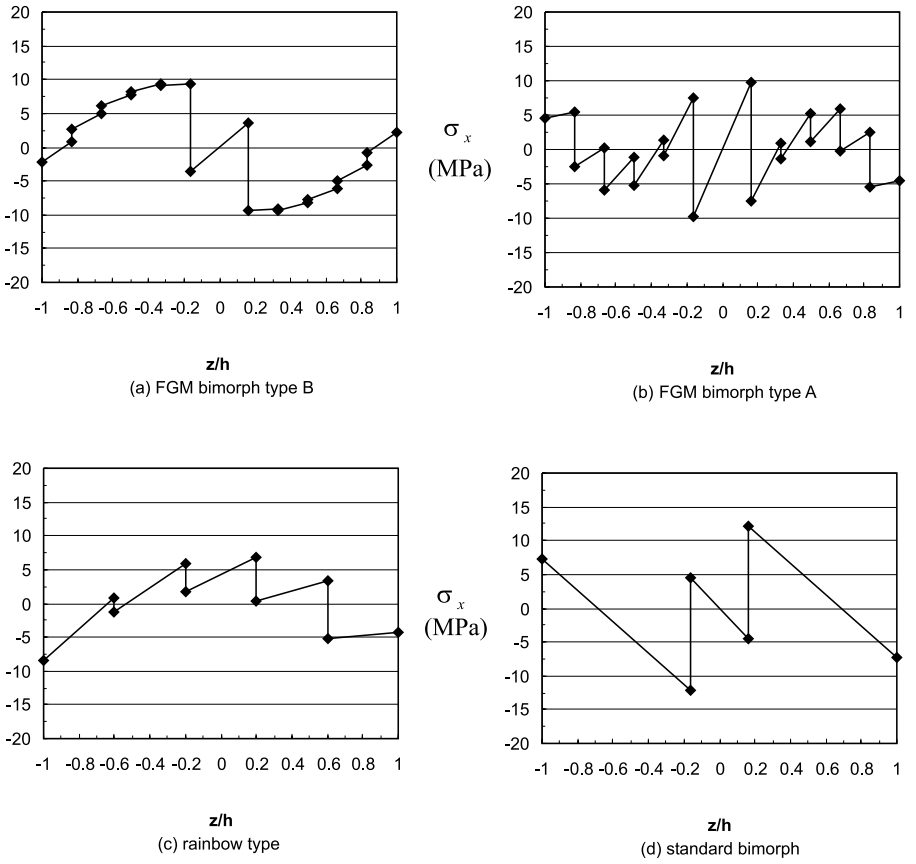

Fig. 6. In-plane stress field profile in the laminated plate throughout the plate thickness (z/h).

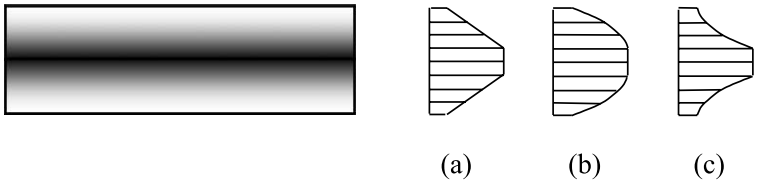

Fig. 7. Material properties distribution (a) linear, (b) convex quadratic, (c) concave quadratic.

(2) Convex Quadratic distribution, Fig. 7(b)

$$\begin{aligned} C_i &= \left[1 - 0.9(-0.25(i-1)+1)^2\right] C_{\mathrm{PZT}}, \\ e_i &= \left[1 - 0.4(-0.25(i-1)+1)^2\right] e_{\mathrm{PZT}}, \end{aligned} \qquad i = 1, 2, \ldots, n, \tag{12}$$

(3) Concave Quadratic distribution, Fig. 7(c)

$$\begin{aligned} C_i &= \left[0.1 + 0.9(0.25(i-1))^2\right] C_{\mathrm{PZT}}, \\ e_i &= \left[0.6 + 0.4(0.25(i-1))^2\right] e_{\mathrm{PZT}}, \end{aligned} \qquad i = 1, 2, \ldots, n. \tag{13}$$

In each case, the properties were arbitrarily chosen as linear, convex quadratic, or concave quadratic functions. The first and last layer of each case have the same electroelastic properties while the middle layers follows their respective distributions. The out-of-plane displacement and maximum stress, σ_x, in the FGM bimorph with these types of distribution of electroelastic properties through the plate thickness have been predicted and are presented in Table 3. The in-plane stress field profile, σ_x, through the thickness of the FGM bimorph for these different distributions of the electroelastic properties are shown in Fig. 8. The out-of-plane displacement of 2 mm for the FGM bimorph with convex quadratic distribution has shown a reduction of about 25% from that of the FGM bimorph with linear distribution, while the in-plane stress is 9.5 MPa which is a reduction of only 3%. The FGM bimorph with concave distribution has the highest out-of-plane displacement at 4 mm, which is an increase of about 30%, while the in-plane stress has also increased to 14.65 MPa, or about 35% higher than found in the FGM bimorph with linear distribution. The stresses generated by the FGM bimorph with concave distribution are even higher than found in the standard bimorph case. It then becomes a design issue of whether the higher deflections of the concave distribution warrant the acceptance of the higher stress levels or whether the reduced stress is more

Table 3
Comparison of analytical results for out-of-plane displacement and maximum σ_x of FGM bimorph clamped plates with three types of distributions of electroelastic properties

Type of FGM microstructure	Linear FGM Fig. 6(a)	Convex quadratic FGM Fig. 6(b)	Concave quadratic FGM Fig. 6(c)
Electric field (V/mm)	1000	1000	1000
Applied voltage (V)	208	208	208
Laminate thickness (mm)	0.5	0.5	0.5
No. of layers	10	10	10
Layer thickness (mm)	0.0416, Au = 0.083	0.0416, Au = 0.083	0.0416, Au = 0.083
Curvature (1/m)	2.15	1.67	3.23
Maximum σ_x (MPa)	9.8	9.5	14.65
Deflection (mm) for plate length of 50 mm	2.7	2.09	4.04

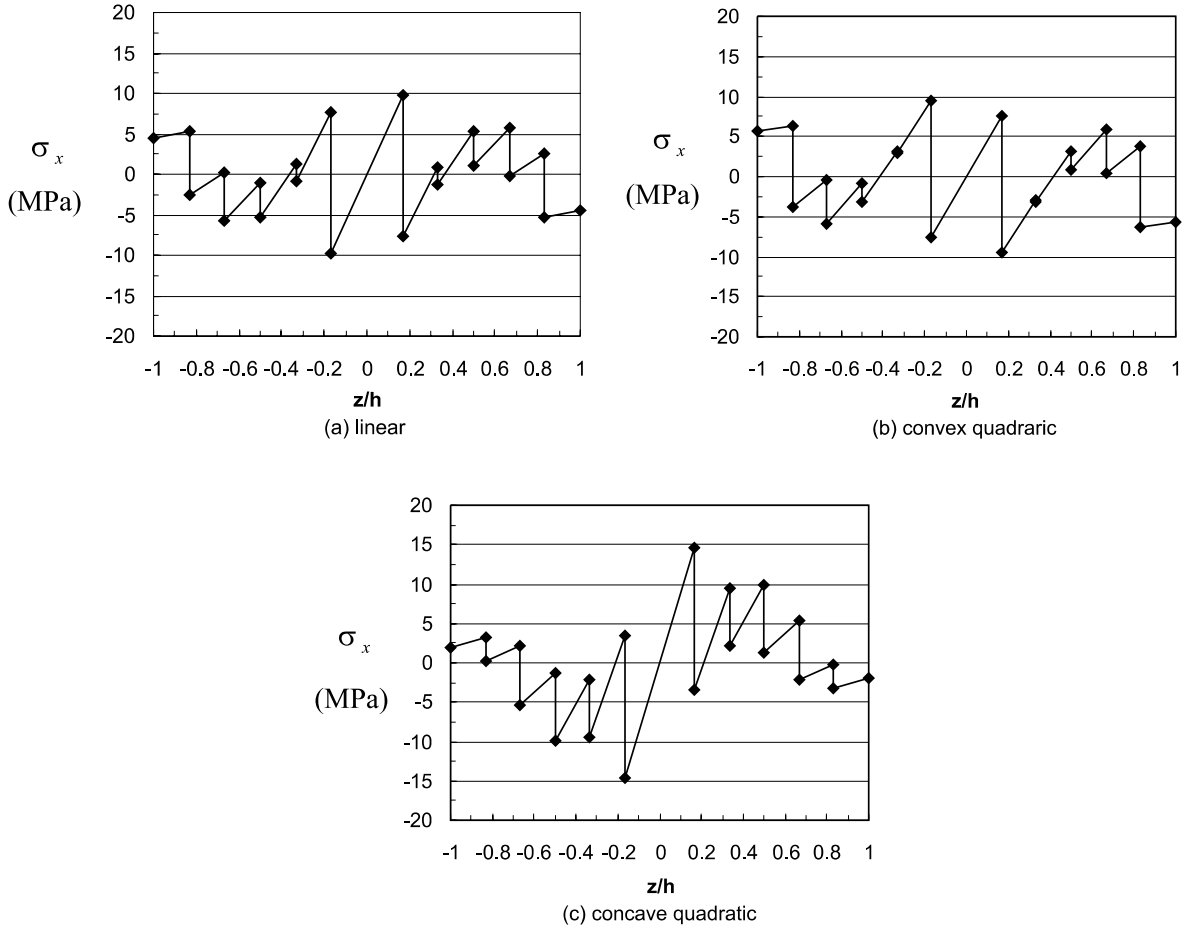

Fig. 8. The in-plane stress field profile in the piezoelectric FGM bimorph plate with different material property distributions.

important. Within these goals of reduced stress and increased displacement, there should be room for optimization.

3.2. Laminated cantilever beam

The reduced lamination theory, 1-D model, is used to solve the stress field and out-of-plane displacement of a cantilever beam where a state of plane stress along the y-axis is also assumed. Two cases are studied, standard bimorph and FGM bimorph. The same dimensions and boundary conditions, except for simplifications from the reduction to beam theory, and electric field as in the previous section are used. The predicted out-of-plane displacements as well as the stress field of the cantilever beam are presented in Table 4. The FGM bimorph gives rise to a higher out-of-plane displacement at 2.7 mm as opposed to the 1.24 mm of the standard bimorph, while the normal stress has been reduced from 7.93 MPa in the standard bimorph to 6.93 MPa in the FGM bimorph. It is noted that the out-of-plane displacements of the cantilever beam are about the same as those of a plate clamped at one end as expected. However, the normal stress of the cantilever beam is less than that of clamped plate as expected due to the additional assumption of plane stress along the y-axis.

Table 4
Comparison of analytical results for out-of-plane displacement and in-plane stress for standard and FGM bimorph cantilever beams

Type of FGM microstructure	Standard bimorph, Fig. 2(a)	Bimorph FGM, Fig. 4(a) type A
Electric field (V/mm)	1000	1000
Applied voltage (V)	208	208
Laminate thickness (mm)	0.5	0.5
No. of layers	2	10
Layer thickness (mm)	0.208, Au = 0.082	0.0416, Au = 0.082
Curvature (1/m)	0.99	2.15
Maximum σ_x (MPa)	7.93	6.93
Deflection (mm) for plate length of 50 mm	1.24	2.7

4. Finite element method analysis

The analytical predictions of piezoelectric laminates need to be verified with some other mathematical computational model such as the FEM. For verification, the FGM bimorphs analyzed analytically in the previous section have also been analyzed using the ANSYS finite element software package. One of the primary reasons for the use of the FEM analysis was to find the shear stress between the layers which could not be found from the lamination model, and also for verification of the analytical results based on the lamination model. The FEM analysis was done on a piezoelectric plate using a 3-D FEM model for the standard bimorph only and also on a piezoelectric cantilever beam case a 2-D FEM model for both the standard bimorph and also the FGM bimorph.

4.1. Piezoelectric plate

A standard bimorph piezoelectric plate was modeled in 3-D to validate the analytical model (Fig. 9). The plate analyzed in this section was assumed to have free edges as opposed to the clamped plate previously

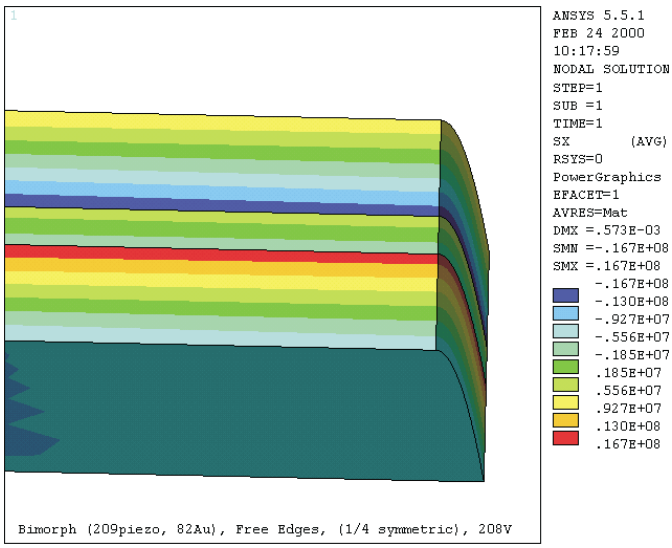

Fig. 9. FEM model for standard piezoelectric bimorph plate.

Table 5
Comparison of ANSYS FEM results with the analytical values based on the lamination theory for a laminated plate with free edges

	Maximum displacement (mm)	σ_x Max (MPa)
Bimorph (analytical)	0.618	12.18
Bimorph (FEM)	0.573	16.7

mentioned. This was done to avoid confusion from the extraneously high stresses induced at the clamped surface near the edges of a wide clamped plate due to the compound curvature produced by the applied electric field. For comparison with this case, the analytical model was also modified to predict the stress and out-of-plane displacement of a free edge plate. The dimensions for the free edged plate as modeled here were an overall length and width of 50 mm. All other dimensions and the applied field were the same as used in the rest of this work. One quarter of the plate was modeled and the symmetry conditions were then applied to model the whole plate, with free edges. The electric field caused the laminate to have an out-of-plane displacement in both x- and y-directions, creating a dome shape in the plate. Table 5 compares the stresses and out-of-plane displacements of a piezoelectric plate of the standard bimorph type based on analytical and FEMs. The out-of-plane displacement of 0.618 mm from the analytical model is very close to the 0.574 mm from the FEM model with only about a 7% difference. The analytical model predicts the stress field found in the FEM model by 25%. The difference in the stress field could be accounted for by considering the moment generated by the out-of-plane displacement that is not included in the current model.

4.2. Laminated cantilever beam

As we mentioned before, two cases are studied here, standard bimorph and FGM bimorph with linear distribution. Models of these cases were made using 2-D FEM with the plane stress condition assumed. The same dimensions, boundary conditions and applied electric field as specified in the previous section for the analytical models, are also used in the FEM models. It is noted that this plane stress assumption (in the FEM work) is for planes stress along the y-axis. (It is further pointed out that due to limitations within the ANSYS package for 2-D analyses, models are created in the x–y plane. For this reason, it was necessary to swap the y- and z-axes so that the former global z-axis becomes the ANSYS y-axis.) Normal stress, σ_x, shear stress, τ_{xz}, and out-of-plane displacement are investigated. The maximum out-of-plane displacement and the stress profile of standard and FGM bimorph are shown in Figs. 10 and 11, respectively, where (A) and (B) are the distribution of the normal stress, σ_x, and that of interlaminar shear stress, τ_{xz}, respectively. The results from the FEM analyses are compared to the analytical results based on the reduced lamination theory for 1-D in Table 6. It can be concluded from Table 6 that the analytical predictions are very close to the FEM results for both standard and FGM bimorph. In the case of standard bimorph, the reduced lamination theory gives rise to 1.24 mm out-of-plane displacement compared to 1.21 mm in the FEM model for a difference of about 7%. In terms of stress field, reduced lamination theory gives a normal stress of 7.93 MPa as opposed to 8.82 MPa by FEM, or a difference of 10%.

The FGM bimorph has a better agreement between the analytical and FEM. In the FEM model of the FGM bimorph, the out-of-plane displacement is 2.68 mm as opposed to 2.7 mm from the analytical model which are almost identical, while the FEM gives a normal stress of 7.4 MPa which is about 6% off of the 6.93 MPa from the analytical model. The magnitude of the shear stress is reduced from 2.65 MPa in the standard bimorph to 1.93 MPa in the FGM bimorph which is a reduction of approximately 30%. The reduction in the shear stress is important, as it is the shear stress, which often leads to the separation of the top and bottom of the bimorph resulting in failure, limiting its life.

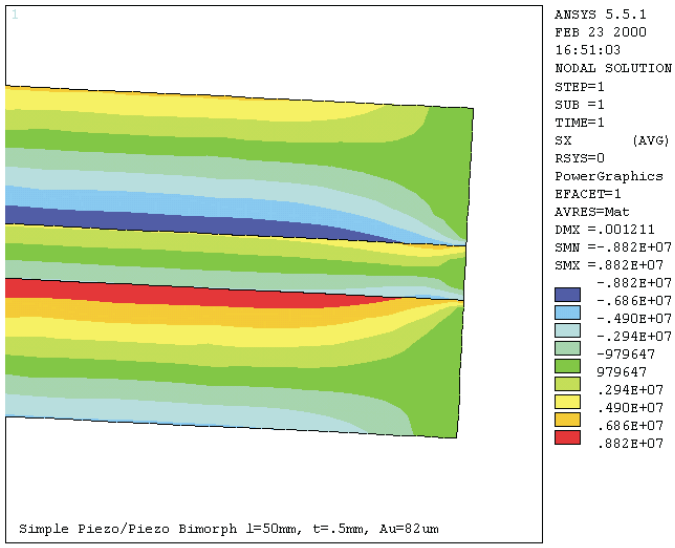

(A)

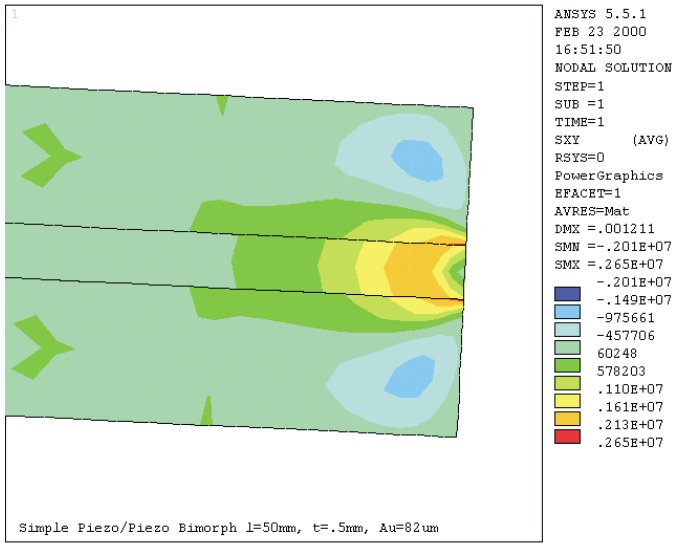

(B)

Fig. 10. FEM model for standard piezoelectric bimorph beam.

5. Conclusion

The CLT developed here for the piezoelectric case provided results that agreed quite well with those found from FEM models. The analytical predictions based on the lamination model for a laminated plate were very close to the 3-D FEM results in terms of out-of-plane displacement, while they were off by about 25% in terms of stress field. These errors in the stress field are believed to be due to moments generated by the plate deflection and future modeling efforts will be aimed at reducing these errors. The analysis of

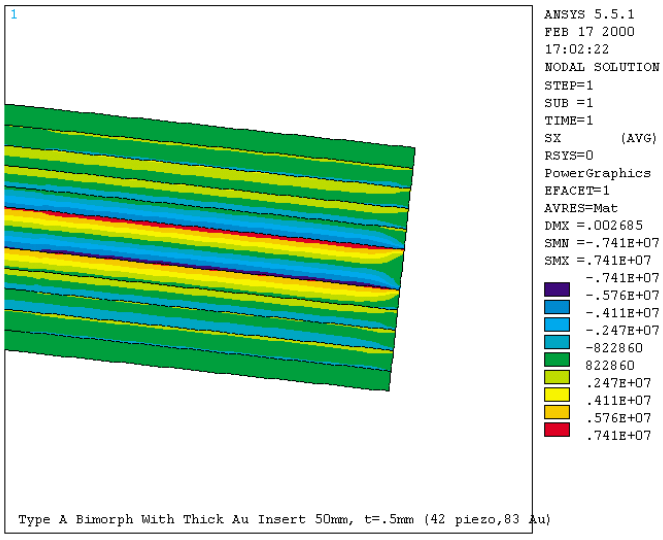

(A)

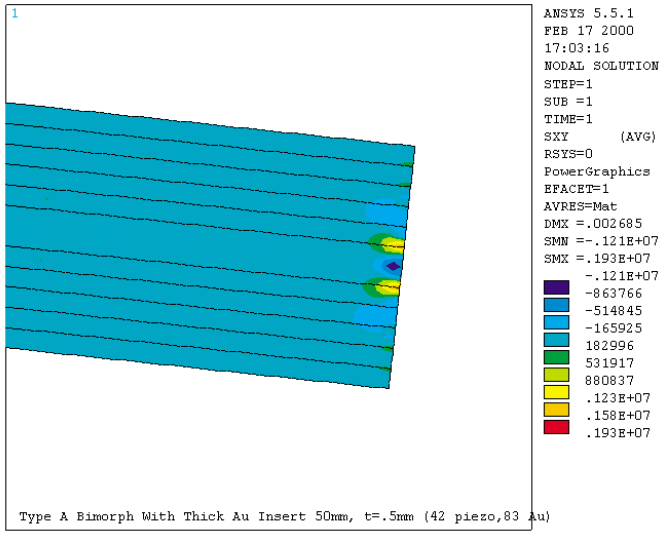

(B)

Fig. 11. FEM model for FGM bimorph beam with linear material property distribution.

Table 6
Comparison of ANSYS 2-D FEM results with the analytical values based on the lamination theory for a laminated cantilever beam

	Tip displacement (mm)	σ_x Max (MPa)	τ_{xz} Max (MPa)
Bimorph (analytical)	1.24	7.93	–
Bimorph (FEM 2-D)	1.21	8.82	2.65
FGM bimorph (analytical)	2.7	6.93	–
FGM bimorph (FEM 2-D)	2.68	7.4	1.93

cantilever beams, using the reduced lamination theory gave very close results when compared to the 2-D FEM models.

Among the different cases of FGM profiles that were investigated, the linear profile has the best performance in terms of higher out-of-plane displacement and moderate stress field, while the concave displacement gave a larger out-of-plane displacement, but at the cost of higher stresses. With this in mind, it will be possible to optimize the material property gradient profile within the FGM to provide higher out-of-plane displacements than standard piezoelectric bimorphs while still maintaining moderate stress levels.

Acknowledgements

The present work was supported in part by a grant from Air Force to the University of Washington (F49620-97-1-0420).

Appendix A. Reduced stiffness and piezoelectric properties for plane stress

The constitutive equation of piezoelectric material, under applied E_z only, are expressed as

$$\begin{Bmatrix} \sigma_x \\ \sigma_y \\ \sigma_z \\ \sigma_{xz} \\ \sigma_{yz} \\ \sigma_{xy} \end{Bmatrix} = \begin{bmatrix} C_{11} & C_{12} & C_{13} & & & \\ & C_{22} & C_{23} & & 0 & \\ & & C_{33} & & & \\ & & & C_{44} & & \\ & \text{sym} & & & C_{55} & \\ & & & & & C_{66} \end{bmatrix} \begin{Bmatrix} \varepsilon_x \\ \varepsilon_x \\ \varepsilon_z \\ \varepsilon_{xz} \\ \varepsilon_{yz} \\ \varepsilon_{xy} \end{Bmatrix} - \begin{bmatrix} 0 & 0 & e_{13} \\ 0 & 0 & e_{23} \\ 0 & 0 & e_{33} \\ 0 & e_{24} & 0 \\ e_{15} & 0 & 0 \\ 0 & 0 & 0 \end{bmatrix} \begin{Bmatrix} 0 \\ 0 \\ E_z \end{Bmatrix} \tag{A.1}$$

the assumption of plane stress in z-axis, where $\sigma_z = \sigma_{xz} = \sigma_{yz} = 0$, leads to

$$\sigma_z = C_{13}\varepsilon_x + C_{23}\varepsilon_y + C_{33}\varepsilon_z - e_{33}E_z = 0. \tag{A.2}$$

The strain in the z-axis then becomes

$$\varepsilon_Z = \frac{1}{C_{33}}\left(-C_{13}\varepsilon_x - C_{23}\varepsilon_y + e_{33}E_z\right) \tag{A.3}$$

and by substituting Eq. (A.3) into Eq. (A.1), the constitutive equations of piezoelectric materials under the applied electric field, and under the assumption of plane stress in z-axis, reduce to

$$\begin{Bmatrix} \sigma_x \\ \sigma_y \\ \sigma_{xy} \end{Bmatrix} = \begin{bmatrix} C_{11} - \frac{C_{13}}{C_{33}}C_{13} & C_{12} - \frac{C_{13}}{C_{33}}C_{23} & 0 \\ C_{12} - \frac{C_{13}}{C_{33}}C_{23} & C_{22} - \frac{C_{23}}{C_{33}}C_{23} & 0 \\ 0 & 0 & C_{66} \end{bmatrix} \begin{Bmatrix} \varepsilon_x \\ \varepsilon_y^0 \\ \gamma_{xy}^0 \end{Bmatrix} - \begin{bmatrix} 0 & 0 & \frac{C_{13}}{C_{33}}e_{33} - e_{13} \\ 0 & 0 & \frac{C_{13}}{C_{33}}e_{33} - e_{23} \\ 0 & 0 & 0 \end{bmatrix} \begin{Bmatrix} 0 \\ 0 \\ E_z \end{Bmatrix}. \tag{A.4}$$

Eq. (A.4) can then be simplified as presented in Eq. (2).

Appendix B. Reduced stiffness and piezoelectric properties for 1-D beam theory model

The constitutive equations of piezoelectric materials, under applied E_z only, and under the assumption of plane stress in z-axis are presented in Eq. (2) as

$$\begin{Bmatrix} \sigma_x \\ \sigma_y \\ \sigma_{xy} \end{Bmatrix} = \begin{bmatrix} \overline{Q}_{11} & \overline{Q}_{12} & 0 \\ \overline{Q}_{21} & \overline{Q}_{22} & 0 \\ 0 & 0 & Q_{66} \end{bmatrix}_i \begin{Bmatrix} \varepsilon_x^0 + z\kappa_x \\ \varepsilon_y^0 + z\kappa_y \\ \gamma_{xy}^0 + z\kappa_{xy} \end{Bmatrix} - \begin{bmatrix} 0 & 0 & \overline{e}_{31} \\ 0 & 0 & \overline{e}_{32} \\ 0 & 0 & 0 \end{bmatrix} \begin{Bmatrix} 0 \\ 0 \\ E_z \end{Bmatrix}, \tag{B.1}$$

where

$$\begin{aligned}\overline{Q}_{ij} &= C_{ij} - \frac{C_{i3}}{C_{33}} C_{j3},\\ \overline{e}_{ij} &= \frac{C_{i3}}{C_{33}} e_{33} - e_{ij};\end{aligned} \tag{B.2}$$

the assumption of further plane stress along the y-axis, where $\sigma_y = \sigma_{xy} = 0$, leads to

$$\sigma_y = \overline{Q}_{12}\varepsilon_x + \overline{Q}_{22}\varepsilon_y - \overline{e}_{32}E_z = 0 \tag{B.3}$$

and the strain in the y-axis then becomes

$$\varepsilon_y = \frac{1}{\overline{Q}_{22}}\left(-\overline{Q}_{12}\varepsilon_x + \overline{e}_{32}E\right) \tag{B.4}$$

and by substituting Eq. (B.4) into Eq. (B.1), the constitutive equations of piezoelectric materials under the applied electric field, and under the assumption of plane stress in z-axis, reduce to

$$\sigma_x = \left(\overline{Q}_{11} - \frac{\overline{Q}_{12}}{\overline{Q}_{22}}\overline{Q}_{12}\right)\varepsilon_x - \left(\frac{\overline{Q}_{12}}{\overline{Q}_{22}}\overline{e}_{32} - \overline{e}_{31}\right)E_z. \tag{B.5}$$

Eq. (B.5) can then be simplified to Eq. (8), where

$$\begin{aligned}E &= \left(\overline{Q}_{11} - \frac{\overline{Q}_{12}}{\overline{Q}_{22}}\overline{Q}_{12}\right) = \left(C_{11} - \frac{C_{13}}{C_{33}}C_{13}\right) - \frac{\left(C_{12} - \frac{C_{13}}{C_{33}}C_{13}\right)^2}{\left(C_{11} - \frac{C_{13}}{C_{33}}C_{13}\right)},\\ e &= \left(\frac{\overline{Q}_{12}}{\overline{Q}_{22}}\overline{e}_{32} - \overline{e}_{31}\right) = \frac{\left(C_{12} - \frac{C_{13}}{C_{33}}C_{13}\right)}{\left(C_{11} - \frac{C_{13}}{C_{33}}C_{13}\right)}\left(\frac{C_{13}}{C_{33}}e_{33} - e_{13}\right) - \left(\frac{C_{13}}{C_{33}}e_{33} - e_{13}\right).\end{aligned} \tag{B.6}$$

References

Chatterjee, D.K., Ghosh, S.K., Furlani, E.P., 1999. Controlled Composition and Crystallographic Changes in Forming Functionally Gradient Piezoelectric Transducer, U. S. Patent, no. 5,900,274.

Crawley, E.F., Anderson, E.H., 1990. Detailed models of piezoceramic actuation of beams. J. Intell. Mater. Sys. Struct. 1, 4–25.

Dunn, M., Taya, M., 1993a. An analysis of piezoelectric composite materials containing ellipsoidal inhomogeneities. Proc. Roy. Soc. Lond. A 443, 265–287.

Dunn, M., Taya, M., 1993b. Micromechanics predictions of the effective electroelastic moduli of piezoelectric composites. Int. J. Solids Struct. 30, 161–175.

Gibson, R.F.,. Principles of Composite Materials and Mechanics, McGraw Hill.

Haertling, G.H., 1994. Rainbow ceramics – a new type of ultra-high-displacement actuator. Am. Ceram. Soc. Bull. 73, 93–96.

Tauchert, T.R., 1992. Piezothermoelastic behavior of a laminated plate. J. Thermal Stresses 15, 25–37.

Taya, M., Lee, J.K., Mori, T., 1997. Dislocation punching from interfaces in functionally-graded materials. Acta materia 45, 2349–2356.

Tzou, H.S., Garde, M., 1989. Theoretical analysis of a multi-layered thin shell coupled with piezoelectric shell actuators for distributed vibration controls. J. Sounds Vibr. 132, 433–450.

Uchino, K., Yoshizaki, M., Kasai, K., Yamamura, H., Sakai, N., Asakura, H., 1987. Monomorph actuators using semiconductive ferroelectrics. Jpn J. Appl. Phys. 26, 1046–1049.

Wu, C.C., Khan, M., Moy, W., 1996. Piezoelectric ceramics with functional gradient: a new application in material design. J. Am. Ceram. Soc. 79, 809–812.

Zhou, Y.S., Tiersten, H.F., 1994. An elastic analysis of laminated composite plates in cylindrical bending due to piezoelectric actuators. Smart Mater. Struct. 3, 255–265.